forests

MDPI

Article

Finite Element Method Simulations and Experiments of Detachments of *Lycium barbarum* L.

Jian Zhao [1,†], Te Ma [2,†], Tetsuya Inagaki [2], Qingyu Chen [1], Zening Gao [1], Lijuan Sun [1], Haoxuan Cai [1], Chao Chen [1], Chuanlin Li [1], Shixia Zhang [1], Satoru Tsuchikawa [2,*] and Jun Chen [1,*]

[1] College of Mechanical and Electronic Engineering, Northwest A&F University, Yangling 712100, China; 2017052634@nwsuaf.edu.cn (J.Z.); 1013137743@nwafu.edu.cn (Q.C.); 2019050925@nwafu.edu.cn (Z.G.); 2020051002@nwafu.edu.cn (L.S.); caihaoxuan1998@nwafu.edu.cn (H.C.); chaochen@nwsuaf.edu.cn (C.C.); 2020055982@nwsuaf.edu.cn (C.L.); 1048912069@nwafu.edu.cn (S.Z.)

[2] Graduate School of Bioagricultural Sciences, Nagoya University, Furo-Cho, Chikusa, Nagoya 464-8601, Japan; mate@agr.nagoya-u.ac.jp (T.M.); inatetsu@agr.nagoya-u.ac.jp (T.I.)

* Correspondence: st3842@agr.nagoya-u.ac.jp (S.T.); chenjun_jdxy@nwsuaf.edu.cn (J.C.); Tel.: +81-52-789-4155 (S.T.); +86-29-8709-1867 (J.C.)

† These authors equally contributed to this work.

Abstract: When harvesting *Lycium barbarum* L., excess amounts of detachments of the half-ripe fruit, unripe fruit, flowers, and leaves significantly affect the yield and adversely affect the subsequent processing, such as drying and grading. Finite element method (FEM) simulations and experiments of detachments were performed to harvest more ripe fruit and less half-ripe fruit, unripe fruit, flowers, and leaves. Three-dimensional (3D) models of the ripe fruit, half-ripe fruit, unripe fruit, flowers, leaves, fruit calyxes (flower calyx), fruit stems (flower stem), and branches were constructed using a 3D scanner, and material mechanics models of the above parts were established based on physical tests with universal testing machines. Detachment simulations and experiments of the ripe fruit, half-ripe fruit, unripe fruit, flowers, and leaves were performed to determine the detachment mechanisms and sequences. The detachment forces of each set of two parts were obtained. The field experiments showed that the detachment force between the fruit and calyx of ripe fruit was the lowest value of these forces, and only the ripe fruit was the first to detach from the calyx when harvesting. The results provided data support on the mechanics properties of wood and the optimization basis for the harvesting method of *L. barbarum*.

Keywords: wood property; *Lycium barbarum* L.; harvesting; reverse engineering modeling; physical test; material mechanics model; FEM simulation; detachment mechanism and sequence

Citation: Zhao, J.; Ma, T.; Inagaki, T.; Chen, Q.; Gao, Z.; Sun, L.; Cai, H.; Chen, C.; Li, C.; Zhang, S.; et al. Finite Element Method Simulations and Experiments of Detachments of *Lycium barbarum* L. *Forests* **2021**, *12*, 699. https://doi.org/10.3390/f12060699

Academic Editor: Angela Lo Monaco

Received: 20 April 2021
Accepted: 27 May 2021
Published: 28 May 2021

1. Introduction

Lycium barbarum L. is a solanaceae *Lycium* deciduous shrub with high added value, and the fruit has high profitability [1–4]. Its ripe fruit after being dried was widely favored by more and more people due to the ingredients, which are beneficial to health, such as a group of *L. barbarum* polysaccharides, which have neuroprotective, anti-oxidant, and immunomodulation functions [3,5]. However, the price of the fruit remains high because *L. barbarum* is harvested manually [4,6], and the harvesting cost accounts for half of the total cost of production, currently. With the increase of the planting area of *L. barbarum*, the problem of labor shortage for the fruit harvesting is becoming increasingly prominent [6]. Thus, it is urgent to design and develop an *L. barbarum* harvester [7–10]. Scholars have developed some prototype harvesters of *L. barbarum* [11–14]. It indicated that half-ripe and unripe fruit were easy to be harvested by mistake [6,11]. Meanwhile, excess amounts of detachments of the half-ripe fruit, unripe fruit, and flowers substantially affect the yield. Hence, it is essential to analyze the detachment mechanisms of *L. barbarum* to achieve the high-efficiency and low-loss harvesting performance. Furthermore, there is

also little research on the wood mechanics properties of *L. barbarum*. This leads to a lack of the key parameters in the analysis and affects the accuracy of the results. In addition, impurities, such as the half-ripe fruit, unripe fruit, flowers, and leaves, significantly affect the subsequent processing, such as the drying and grading [15]. Therefore, it is crucial to investigate the detachment sequences of *L. barbarum* to harvest more ripe fruit and less half-ripe fruit, unripe fruit, flowers, and leaves. The essence of detachment forces was the strength of plant attachments. The branch-to-stem diameter ratio affected the strength of plant attachments [16,17]. In addition, the picking patterns have a significant effect on the detachment forces [18,19]. Thus, dividing the ripe fruit, half-ripe fruit, unripe fruit, flowers, and leaves of *L. barbarum* into different plant parts according to the materials was more accurate to analyze the detachment mechanisms and sequences of *L. barbarum*. With the development of the reverse engineering technology, it was easy to obtain accurate three-dimensional (3D) models. Modeling each plant part using the reverse engineering technology was more conducive to simulation analyses accurately. Additionally, the material mechanics parameters of different plant parts were different. It was necessary to establish material mechanics models through physical tests [20,21]. On this basis, it was expected to access the detachment mechanisms and sequences of *L. barbarum* by performing finite element method (FEM) simulations and experiments.

In this study, to harvest more ripe fruit and less half-ripe fruit, unripe fruit, flowers, and leaves, 3D models of the ripe fruit, half-ripe fruit, unripe fruit, flower, leaf, fruit calyxes (flower calyx), fruit stems (flower stem), and branches were constructed using a 3D scanner, and material mechanics models of the above parts were established based on physical tests with universal testing machines. FEM simulations and experiments of detachments of the ripe fruit, half-ripe fruit, unripe fruit, flowers, and leaves were performed to determine the detachment mechanisms and sequences of *L. barbarum*. The detachment forces of each set of two parts were also obtained. Such findings provided data support on the mechanics properties of wood and the optimization basis for the harvesting method of *L. barbarum*.

2. Materials and Methods

2.1. Reverse Engineering Modeling Using the 3D Scanner

The more realistic the 3D models are, the more accurate the results of subsequent detachment simulations based on FEM will be. Reverse engineering modeling was used to obtain accurate 3D models using the 3D scanner (type: HandySCAN 700; precision: 0.03 mm; manufactured by Creaform Shanghai Co., Ltd., Shanghai, China). The material mechanics properties differ for different plant parts, affecting the results of detachment simulations and experiments. The ripe fruit, half-ripe fruit, and unripe fruit could be divided into four parts (i.e., the fruit, fruit calyx, fruit stem, and branch), as shown in Figure 1a–c. As shown in Figure 1d, the flower could be divided into four parts (i.e., the flower, flower calyx, flower stem, and branch). As shown in Figure 1e, the leaf could be divided into two parts (i.e., the leaf and branch). The creations of the 3D models of the ripe fruit, half-ripe fruit, unripe fruit, flowers, leaves, fruit calyxes (flower calyx), fruit stems (flower stem), and branches included calibrating, configuring, attaching marking points, scanning the orientation point, scanning the sample, meshing, and rendering in the software (type: Vxelements 3D software version-6.1; manufactured by Creaform Inc., Lévis, Canada). To better display the 3D models, their surfaces were rendered with the color blue. There were some defects in the surfaces due to the shade and illumination during the scanning process. The defects were corrected based on the morphology method and rendered with the color yellow in the 3D models.

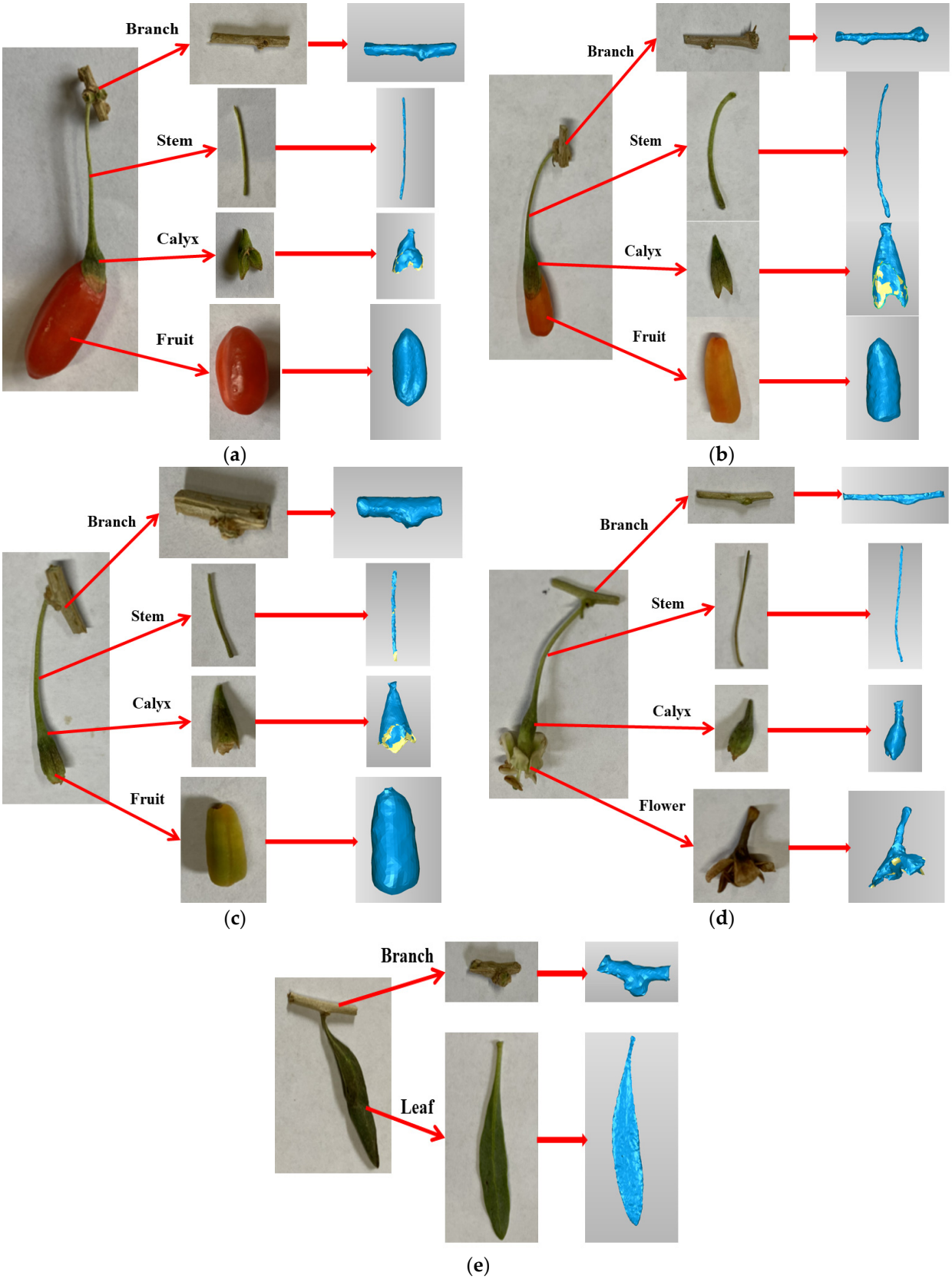

Figure 1. The photos and 3D models of the ripe fruit (**a**), half-ripe fruit (**b**), unripe fruit (**c**), flowers (**d**), and leaves (**e**).

2.2. Physical Tests Using Universal Testing Machines

The density, elastic modulus, and Poisson ratio are essential parameters for the detachment simulations. The densities of the plant parts were calculated by measuring the masses and volumes of the corresponding parts. Two electronic scales (type: Professional digital jewelry scale 8028-series; measurement range: 0–100 g; precision: 0.001 g; manufactured by Shenzhen Diheng Electronics Co., Ltd., Shenzhen, China and type: SA-120; measurement range: 0–120 g; precision: 0.0002 g; manufactured by Shinko Denshi Co., Ltd., Tokyo, Japan) were used to measure the masses. Two electronic vernier calipers (type: AIRAJ second-generation product; measurement range: 0–300 mm; precision: 0.01 mm; manufactured by Qingdao Yigou Hardware Tools Co., Ltd., Qingdao, China and type: CD-15APX; measurement range: 0–150 mm; precision: 0.01 mm; manufactured by Mitutoyo Corporation, Kanagawa, Japan) were used to obtain the measurements. The volumes could be calculated according to the obtained measurements. The Poisson ratios were obtained from relevant references. However, the elastic moduli should be calculated from the stress–strain curves obtained in the physical tests. Hence, two electronic universal testing machines (type: DDL10; max testing force: 10 kN; manufactured by Sinotest Equipment Co., Ltd., Changchun, China and type: AG-1; max testing force: 100 kN; manufactured by Shimadzu Corporation, Kyoto, Japan) were used to perform all physical tests. The cutting surfaces of the samples were polished before the tests. Meanwhile, in order to get more accurate stress–strain curves, compression or tensile tests should be selected according to the samples. Therefore, physical tests of the ripe fruit, half-ripe fruit, unripe fruit, flower, leaf, fruit calyxes (flower calyx), fruit stems (flower stem), and branches were conducted.

2.3. Establishing the Material Mechanics Models

2.3.1. Densities

The more realistic the hypothetical shapes are, the more accurate the densities are when calculating the volumes of the plant parts. Since the shapes of the ripe fruit, half-ripe fruit, and unripe fruit are similar to an ellipsoid, the volumes of the ripe fruit, half-ripe fruit, and unripe fruit were calculated using the following Equation (1) of an ellipsoid.

$$V = \frac{4}{3}\pi abc \tag{1}$$

where V is the volume of the sample, mm^3; a, b, and c are half of the length of each axis of the ellipsoid-shaped sample, mm.

The flower is cone-shaped; thus, the volume of the flower was calculated using the following Equation (2) of a cone.

$$V = \frac{1}{3}\pi R^2 h \tag{2}$$

where R is the bottom radius of the cone-shaped sample, mm; h is the height of the cone-shaped sample, mm.

The leaf is cuboid-shaped; thus, the volume of the leaf was calculated using the following Equation (3) of a cuboid.

$$V = abh \tag{3}$$

where a is the length of the cuboid-shaped sample, mm; b is the width of the cuboid-shaped sample, mm; h is the height of the cuboid-shaped sample, mm.

The calyxes of the ripe fruit, half-ripe fruit, unripe fruit, and flowers are cone-shaped; thus, the volumes of these parts were calculated using the Equation (2) of a cone. The stems of the ripe fruit, half-ripe fruit, unripe fruit, and flowers and the branches of the ripe fruit, half-ripe fruit, unripe fruit, flowers, and leaves are similar to a cylinder. The volumes of these parts were calculated using the following Equation (4) of a cylinder.

$$V = \pi R^2 h \tag{4}$$

where R is the bottom radius of the cylinder-shaped sample, mm; h is the height of the cylinder-shaped sample, mm.

The densities of all plant parts were calculated using the following Equation (5). The results are listed in Table 1.

$$\rho = \frac{m}{V} \tag{5}$$

where ρ is the density of the sample, t/mm^3; m is the mass of the sample, t.

Table 1. The material mechanics parameters of the plant parts.

Item	Density (t/mm^3)	Elastic Modulus (MPa)	Poisson Ratio
The ripe fruit	9.3339×10^{-10}	1.3440×10^{-1}	0.4000
The half-ripe fruit	9.6742×10^{-10}	4.0970×10^{-1}	0.4000
The unripe fruit	8.5822×10^{-10}	4.4694	0.4000
The flower	3.1461×10^{-11}	1.5500×10^{-1}	0.4500
The leaf	5.3178×10^{-10}	4.2090	0.4500
The calyx of ripe fruit	3.3684×10^{-11}	3.5500×10^{-2}	0.4200
The calyx of half-ripe fruit	4.3356×10^{-11}	1.6100×10^{-2}	0.4200
The calyx of unripe fruit	1.5180×10^{-10}	8.8500×10^{-2}	0.4200
The calyx of flower	8.3132×10^{-11}	1.2900×10^{-2}	0.4200
The stem of ripe fruit	2.4618×10^{-9}	8.2110	0.3800
The stem of half-ripe fruit	2.1556×10^{-9}	1.1322	0.3800
The stem of unripe fruit	2.2060×10^{-9}	4.9444	0.3800
The stem of flower	1.5778×10^{-9}	3.2611	0.3800
The branch of ripe fruit	4.1148×10^{-10}	4.2564×10^{2}	0.3000
The branch of half-ripe fruit	1.6544×10^{-9}	1.9119×10^{2}	0.3000
The branch of unripe fruit	1.0988×10^{-9}	2.5738×10^{2}	0.3000
The branch of flower	1.2096×10^{-9}	5.6472×10^{2}	0.3000
The branch of leaf	9.9668×10^{-10}	4.5531×10^{2}	0.3000

2.3.2. Elastic Moduli

The stresses and strains were calculated based on the following Equations (6) and (7) and the references [3,22,23]:

$$\sigma = \frac{F}{A_0} \tag{6}$$

$$\varepsilon = \frac{\Delta l}{l_0} \tag{7}$$

where σ is the stress of the sample, MPa; F is the load of the test, N; A_0 is the cross-sectional area of the sample, mm^2; ε is the strain of the sample, mm·mm^{-1}; Δl is the change in the length of the sample, mm; l_0 is the nominal length of the sample, mm.

The elastic modulus is defined as the following Equation (8) based on the references [3,22,23]:

$$E = \frac{\sigma}{\varepsilon} \tag{8}$$

where E is the elastic modulus of the sample, MPa.

The load of the test and the change in the length of the sample were obtained from tests with the universal testing machines. The nominal length of the sample was measured using the electronic vernier calipers. However, the cross-sectional area of the sample should be determined based on the sample shapes. The mean values of the largest and smallest ellipse area of the ripe fruit, half-ripe fruit, and unripe fruit were considered the cross-sectional area of the sample. The mean value of the largest and smallest round area of the flower was considered the cross-sectional area of the sample. The mean value of the largest and smallest rectangle area of the leaf was considered the cross-sectional area of the sample. The mean values of the largest and smallest round area of the calyxes of the ripe fruit, half-ripe fruit, unripe fruit, and flowers were considered the cross-sectional area of the sample. The mean values of the largest and smallest round area of the stems of

the ripe fruit, half-ripe fruit, unripe fruit, and flowers and the branches of the ripe fruit, half-ripe fruit, unripe fruit, flowers, and leaves were considered the cross-sectional area of the sample. Therefore, the elastic moduli of all plant parts were calculated based on the stress–strain curves and are listed in Table 1.

2.3.3. Poisson Ratio

The Poisson ratio is the ratio of the absolute value of the transverse positive strain to the axial positive strain when a material is under a unidirectional compression or tension test, also known as a transverse deformation coefficient, which is an elastic constant reflecting the transverse deformation of a material [24]. According to the previous studies, the Poisson ratios of many materials have been measured. Since the Poisson ratio has little effect on the simulation result, the usual practice is to assume the Poisson ratio of the material according to the Poisson ratio of the similar material obtained previously. Therefore, the Poisson ratios of all plant parts were assumed and obtained from the references [3,25–30] and are listed in Table 1.

2.4. Detachment Simulations Based on FEM

After obtaining the material mechanics parameters, the FEM simulations results could be analyzed to access the detachment mechanisms of the ripe fruit, half-ripe fruit, unripe fruit, flowers, and leaves theoretically. The simulations were conducted using the Abaqus software. The 3D models were inputted into the Part module. The material mechanics parameters (i.e., the density, elastic modulus, and Poisson ratio) of the plant parts (Table 1) were inputted into the Property module. The velocity was chosen in the predefined field type, and the definition was translational only in the Load module. Each branch was selected as the embedded option, and the mass centers of the above parts were assigned a vertical downward velocity in this module. The 3D models of the ripe fruit, half-ripe fruit, unripe fruit, flowers, and leaves were meshed in the Mesh module, as shown in Figure 2a, Figure 3a, Figure 4a, Figure 5a, and Figure 6a, respectively. Many grids were used to make up the models. Every grid was green, and the boundaries between the grids were black.

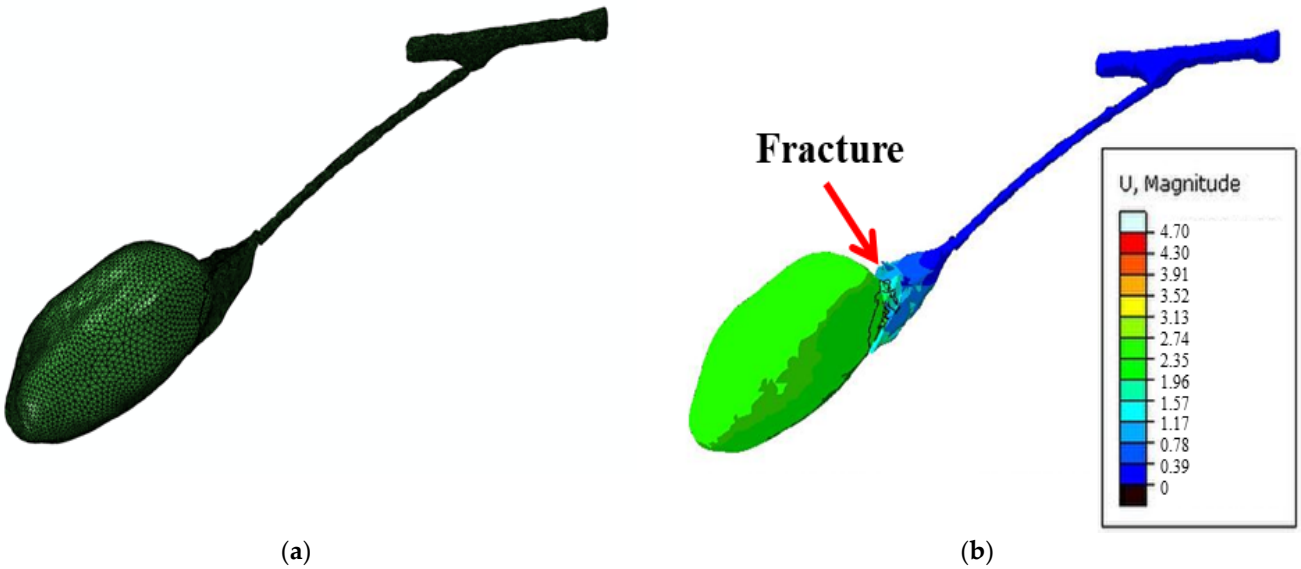

Figure 2. The meshed model (**a**) and the result (**b**) of the ripe fruit in the detachment simulation.

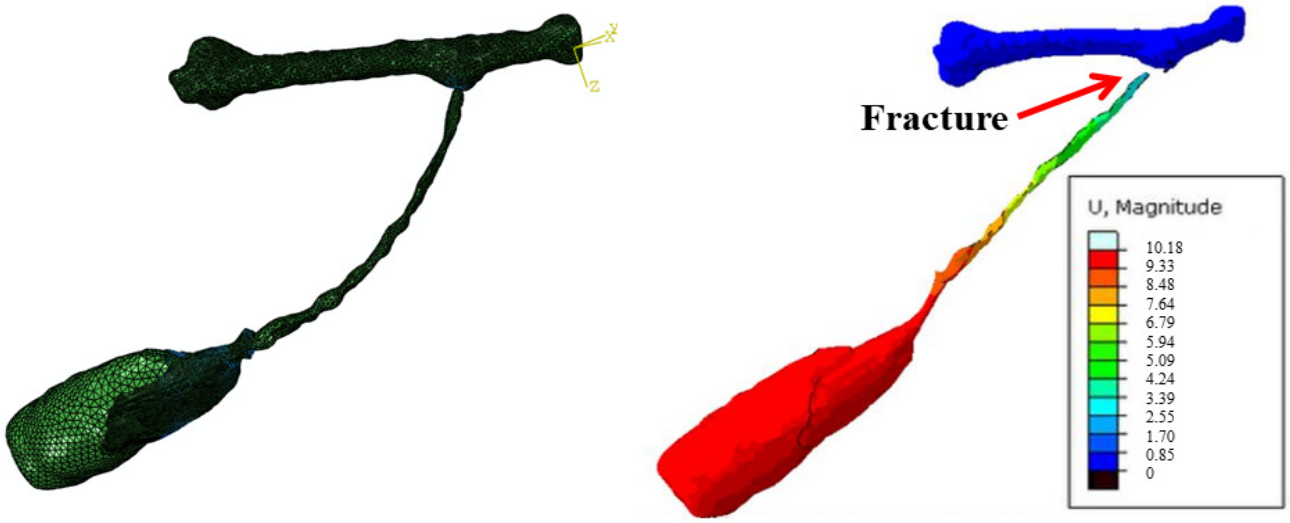

(**a**) (**b**)

Figure 3. The meshed model (**a**) and the result (**b**) of the half-ripe fruit in the detachment simulation.

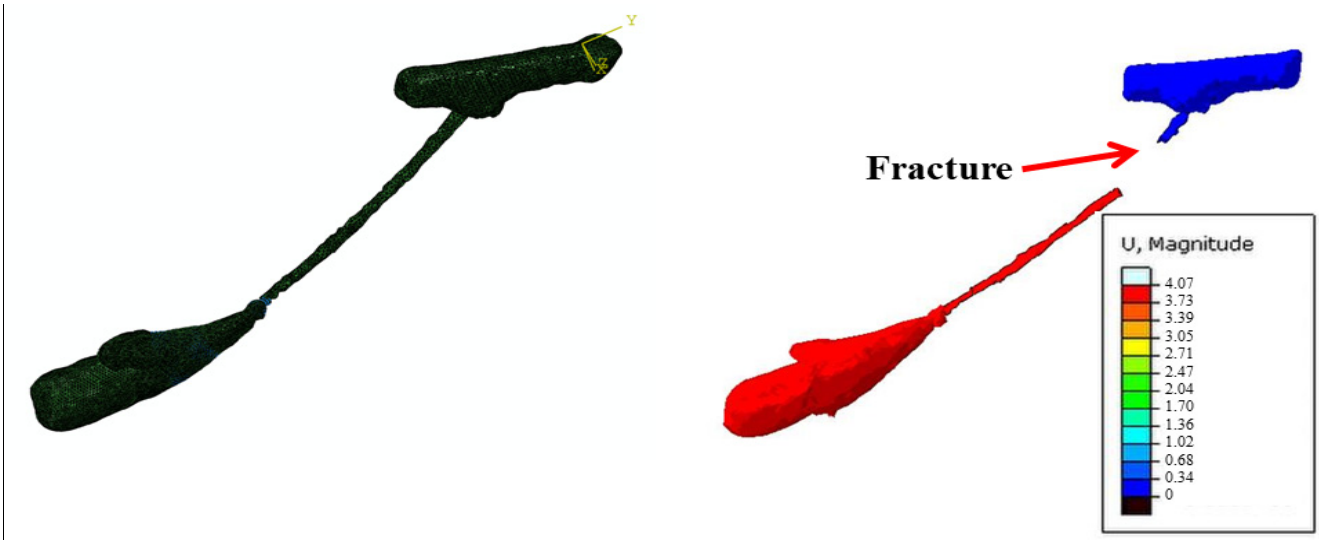

(**a**) (**b**)

Figure 4. The meshed model (**a**) and the result (**b**) of the unripe fruit in the detachment simulation.

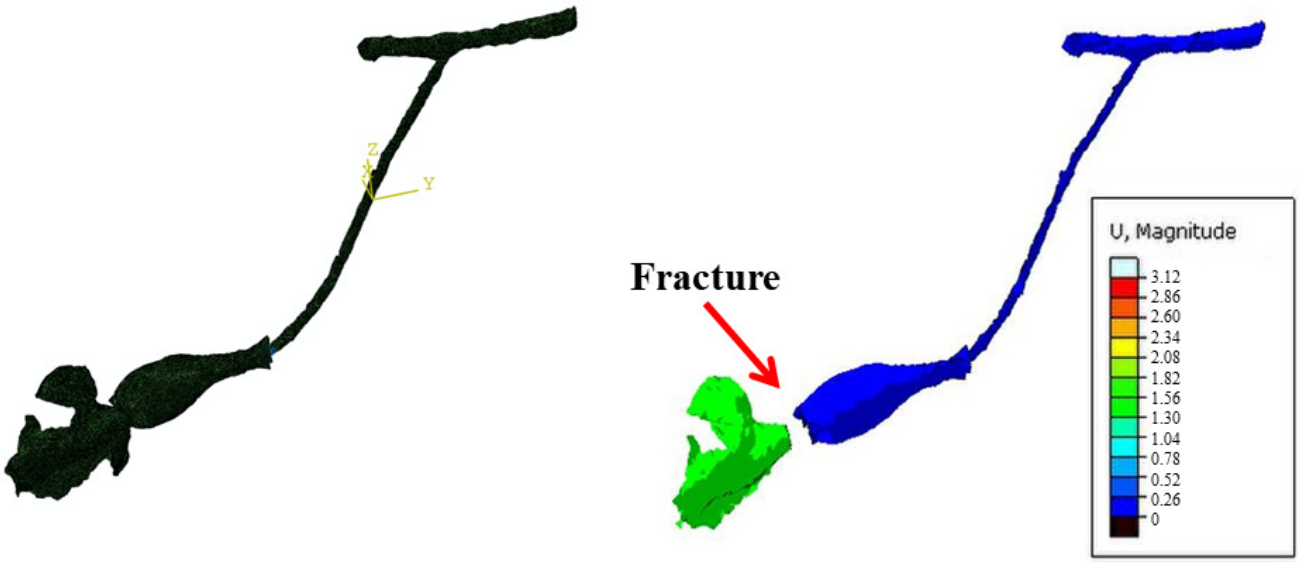

(**a**) (**b**)

Figure 5. The meshed model (**a**) and the result (**b**) of the flower in the detachment simulation.

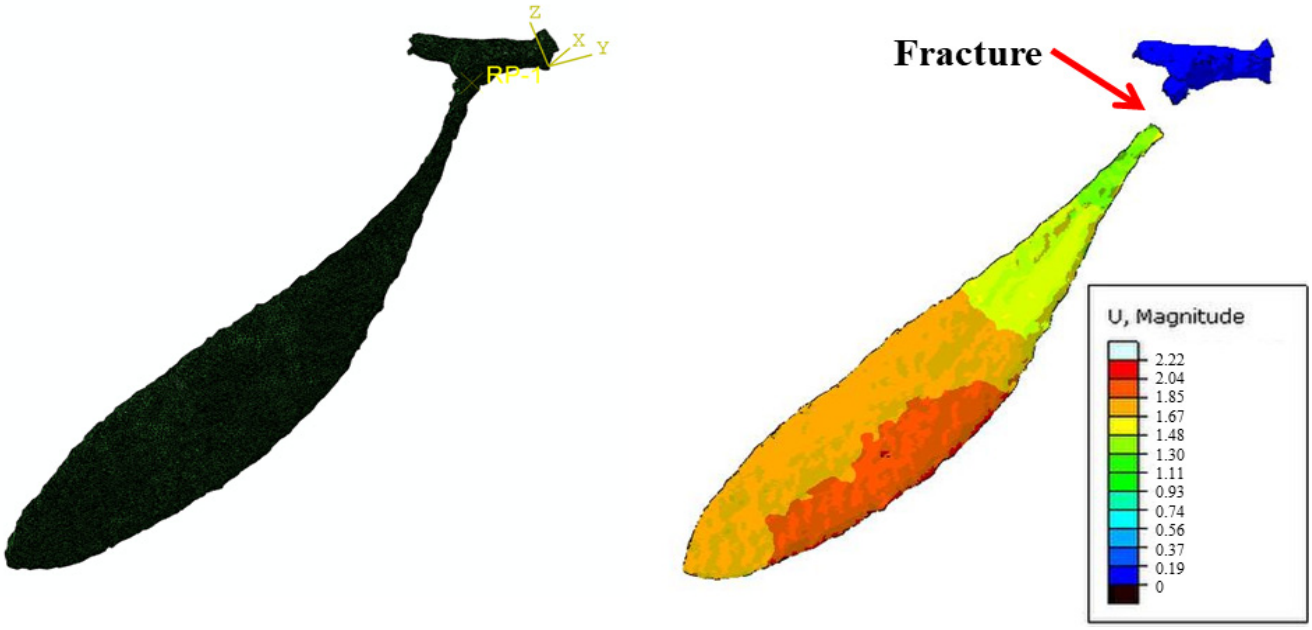

(**a**) (**b**)

Figure 6. The meshed model (**a**) and the result (**b**) of the leaf in the detachment simulation.

3. Results

3.1. Analyses of Detachment Simulations

The analyses and post-processing of the ripe fruit, half-ripe fruit, unripe fruit, flowers, and leaves were performed in the Visualization module. The simulation results of the ripe fruit, half-ripe fruit, unripe fruit, flowers, and leaves are shown in Figure 2b, Figure 3b, Figure 4b, Figure 5b, and Figure 6b, respectively. The magnitude was the relative displacement comparing to the initial state and selected as the display option of simulation results. The greater the magnitude value, the greater the relative displacement. The relative displacements of each part during the detachment progress were displayed in real time. The first fracture of the ripe fruit occurred between the fruit and calyx. That of the half-ripe fruit occurred between the stem and branch mostly. That of the unripe fruit occurred

between the stem and branch. That of the flower occurred between the flower and calyx mostly. That of the leaf occurred between the leaf and branch.

3.2. Verification Using Field Experiments

Field experiments were conducted to verify the accuracy of the detachment simulations results of the ripe fruit, half-ripe fruit, unripe fruit, flowers, and leaves. A digital display tensile force meter (type: HP-30; measurement range: 0–30 N; precision: 0.01 N; manufactured by Yueqing Aidebao Instrument Co., Ltd., Yueqing, China) was used to measure the detachment forces. Each experiment was repeated ten times to eliminate random errors. As shown in Table 2, the detachment forces of each two parts were obtained, and the unit was N. The mean values and standard deviations were also obtained. The standard deviations reflected the degree of dispersion of a dataset. According to the standard deviations, the mean values of each force were valid, and the force value was evenly distributed for the same detachment force. To better display the detachment sequences, representative samples with the similar time dimension were selected for the comparison. The detachment experiments results of the ripe fruit, half-ripe fruit, and unripe fruit are shown in Figure 7 and that of the flowers and leaves are shown in Figure 8.

Table 2. The detachment forces of *L. barbarum*.

Item	Maximum Value	Minimum Value	Mean Value	Standard Deviation
The first detachment force of ripe fruit (R1)	1.26	0.32	0.62	0.33
The second detachment force of ripe fruit (R2)	2.54	0.57	1.21	0.58
The first detachment force of half-ripe fruit (H1)	3.35	0.16	1.08	0.86
The second detachment force of half-ripe fruit (H2)	3.62	0.70	1.51	0.82
The first detachment force of unripe fruit (U1)	2.15	0.38	1.13	0.52
The second detachment force of unripe fruit (U2)	3.16	1.32	2.10	0.55
The first detachment force of flowers (F1)	1.10	0.49	0.75	0.20
The first detachment force of leaves (L1)	3.93	1.47	2.94	0.85

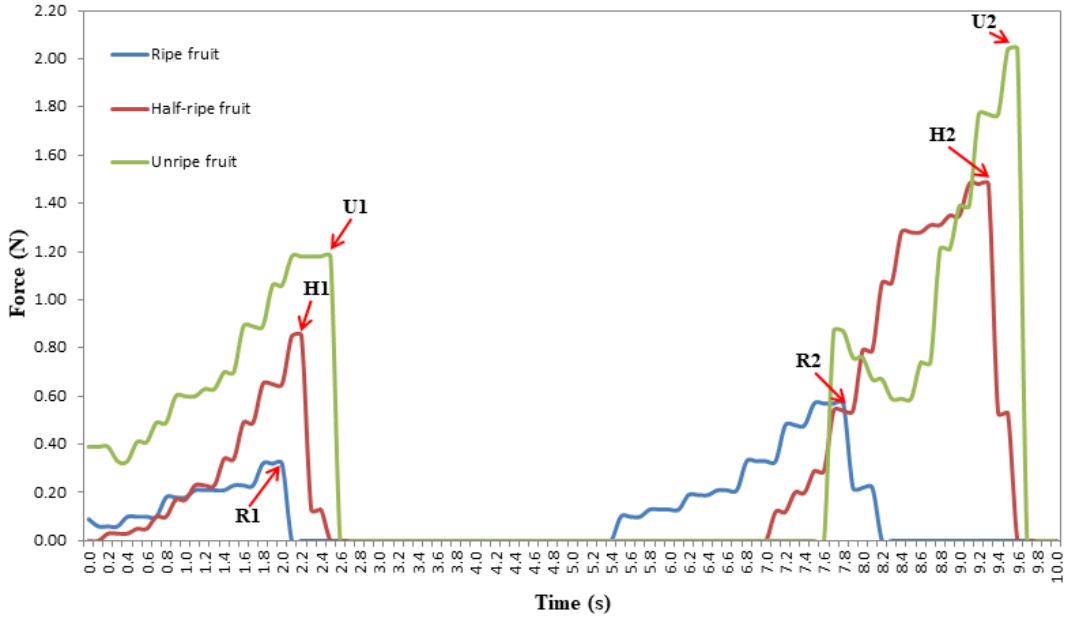

Figure 7. The detachment experiments results of the ripe fruit, half-ripe fruit, and unripe fruit.

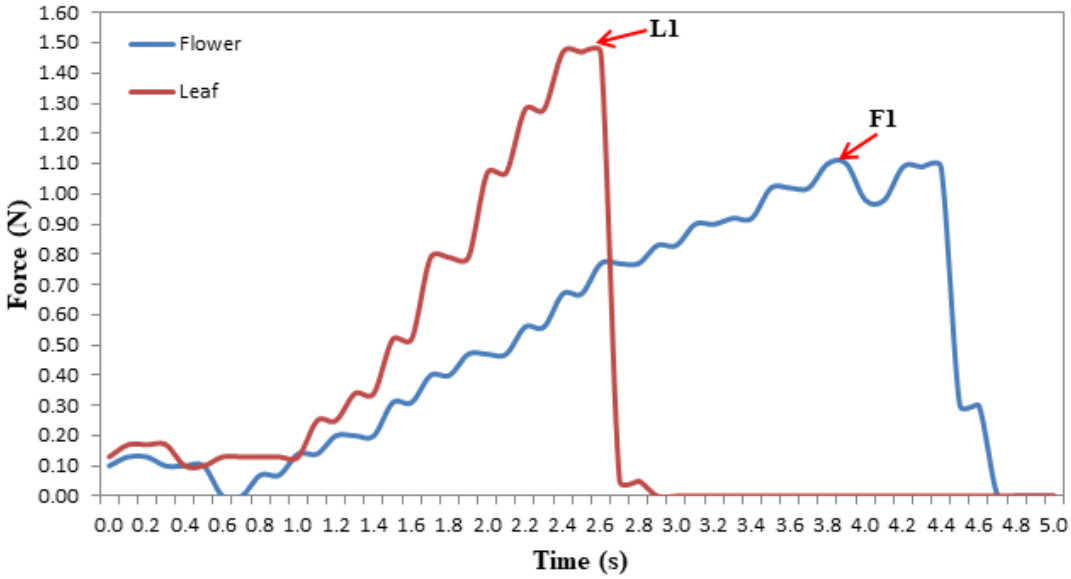

Figure 8. The detachment experiments results of the flowers and leaves.

4. Discussion

Based on the field experiments results, as shown in Figure 7; Figure 8, the detachment mechanisms and sequences of the ripe fruit, half-ripe fruit, unripe fruit, flowers, and leaves were determined. To be specific, the ripe fruit fractured first between the fruit and calyx, second between the stem and branch, and the stem fractured last. Mostly, the half-ripe fruit fractured first between the stem and branch, second between the fruit and calyx, and the stem fractured last. The unripe fruit fractured first between the stem and branch, second between the fruit and calyx, and the stem fractured last. The flower fractured first between the flower and calyx mostly, the stem fractured first in some cases, and it fractured first between the stem and branch least often. The leaves fractured between the leaf and branch. The field experiments results were consistent with the simulations results. This also showed that the established material mechanics models of the plant parts were accurate.

As shown in Table 2, it indicated that the detachment force between the fruit and calyx of ripe fruit was the lowest value of these forces. The detachment forces of the ripe fruit, half-ripe fruit, unripe fruit, flowers, and leaves were also distributed stably. Therefore, only the ripe fruit was the first to detach from the calyx when harvesting. Scholars who have designed the *L. barbarum* harvesters also proposed that impurities, such as unripe fruit and flowers, affected the comprehensive harvesting performance [1,2,4,6,11,15]. Based on the obtained results, it was expected to design and develop a *L. barbarum* harvester, which could harvest more ripe fruit and less half-ripe fruit, unripe fruit, flowers, and leaves. When designing the harvester, the component forces of the harvester mechanism should be integrated to form the resultant force, firstly. Then, the resultant force was compared with the detachment forces. As long as the resultant force was greater than the detachment force between the fruit and calyx of ripe fruit and less than the other detachment forces, it was expected to achieve the high-efficiency and low-loss harvesting performance.

Furthermore, codominant stems were easy to split apart compared with branches that were small relative to stem size [16]. It illustrated that the detachment forces of the ripe fruit, half-ripe fruit, unripe fruit, flowers, and leaves were different. The strength of attachment was the major factor that affected the detachment force [16,17]. Hu et al. proposed that studies of the detachment force were a basis to design a fruit harvester. It revealed that the detachment forces of different forms were different [31]. It was consistent with the obtained results in this study. The results in this study provided data support on mechanics properties of wood and the optimization basis for the harvesting method of *L. barbarum*. In addition, it indicated that the tension was the dominant factor during the

detachment process [32]. Based on the tension, the detachment mechanisms and sequences of *L. barbarum* were determined, and the detachment forces of each two parts were also obtained in this study. It also showed that harvesting patterns were also critical for the efficient harvesting from references [18,19,32]. Especially, there were four picking methods, i.e., the horizontal pull, vertical tension, bending, and twisting [32]. Therefore, based on the obtained results in this study, further study is required to determine which harvesting patterns (i.e., the pull, bend, and torsion) are more efficient for harvesting *L. barbarum*.

5. Conclusions

In this study, to harvest more ripe fruit and less half-ripe fruit, unripe fruit, flowers, and leaves, FEM simulations and experiments of detachments of *L. barbarum* were conducted to determine the detachment mechanisms and sequences. Firstly, 3D models of the ripe fruit, half-ripe fruit, unripe fruit, flowers, leaves, fruit calyxes (flower calyx), fruit stems (flower stem), and branches were constructed using the 3D scanner. Then, material mechanics models of the above parts were established based on physical tests with universal testing machines. Lastly, detachment simulations and experiments of the ripe fruit, half-ripe fruit, unripe fruit, flowers, and leaves were performed to determine the detachment mechanisms and sequences. The detachment forces of each set of two parts were also obtained. The field experiments showed that the detachment force between the fruit and calyx of ripe fruit was the lowest value of these forces, and only the ripe fruit was the first to detach from the calyx when harvesting. According to the obtained results, it was expected to design and develop a *L. barbarum* harvester, which could harvest more ripe fruit and less half-ripe fruit, unripe fruit, flowers, and leaves. When designing the harvester, the component forces of the harvester mechanism should be integrated to form the resultant force, firstly. Then, the resultant force was compared with the detachment forces. As long as the resultant force was greater than the detachment force between the fruit and calyx of ripe fruit and less than the other detachment forces, it was expected to achieve the high-efficiency and low-loss harvesting performance. The results could provide data support on the mechanics properties of wood and the optimization basis for the harvesting method of *L. barbarum*. Further study is required to determine which harvesting patterns (i.e., the pull, bend, and torsion) are more efficient for harvesting *L. barbarum* based on the knowledge earned in this study.

Author Contributions: Conceptualization, J.Z., T.M., T.I., S.T. and J.C.; methodology, J.Z., T.M., T.I., S.T. and J.C.; software, J.Z., T.M., L.S. and H.C.; validation, J.Z., T.M., Q.C., Z.G., C.C. and C.L.; investigation, J.Z., T.M., Q.C., Z.G. and S.Z.; writing—original draft preparation, J.Z.; writing—review and editing, T.M., T.I., S.T. and J.C.; visualization, J.Z., T.M., T.I., S.T. and J.C.; funding acquisition, J.C. All authors have read and agreed to the published version of the manuscript.

Funding: This research and APC were funded by the National Key Research and Development Program of China, grant number 2018YFD0701102. The authors also appreciate the financial support provided by the China Scholarship Council.

Conflicts of Interest: The authors declare no conflict of interest.

References

1. Xu, L.; Chen, J.; Wu, G.; Yuan, Q.; Ma, S.; Yu, C.; Duan, Z.; Xing, J.; Liu, X. Design and operating parameter optimization of comb brush vibratory harvesting device for wolfberry. *Trans. CSAE* **2018**, *34*, 75–82. [CrossRef]
2. Zhang, Z.; Xiao, H.; Ding, W.; Mei, S. Machanism simulation analysis and prototype experiment of *Lycium barbarum* harvest by vibration mode. *Trans. CSAE* **2015**, *31*, 20–28. [CrossRef]
3. Zhao, J.; Sugirbay, A.; Chen, Y.; Zhang, S.; Liu, F.; Bu, L.; Chen, Y.; Wang, Z.; Chen, J. FEM explicit dynamics simulation and NIR hyperspectral reflectance imaging for determination of impact bruises of *Lycium barbarum* L. *Postharvest Biol. Technol.* **2019**, *155*, 102–110. [CrossRef]
4. Wang, Y.; Chen, Y.; Han, B.; Chen, J. Research on laws of wolfberry dropping based on high-speed camera. *J. Agric. Mech. Res.* **2018**, *40*, 166–170. [CrossRef]
5. Amagase, H.; Farnsworth, N.R. A review of botanical characteristics, phytochemistry, clinical relevance in efficacy and safety of *Lycium barbarum* fruit (Goji). *Food Res. Int.* **2011**, *44*, 1702–1717. [CrossRef]

6. Chen, J.; Zhao, J.; Chen, Y.; Bu, L.; Hu, G.; Zhang, E. Design and experiment on vibrating and comb brushing harvester for *Lycium barbarum*. *Trans. CSAM* **2019**, *50*, 152–161. [CrossRef]
7. So, J.D. Vibration characteristics of boxthorn (*Lycium chinense* Mill) branches. *Appl. Eng. Agric.* **2001**, *17*, 755–760. [CrossRef]
8. So, J.D. Vibratory harvesting machine for boxthorn (*Lycium chinense* Mill) berries. *Trans. ASAE* **2003**, *46*, 211–221. [CrossRef]
9. Zhang, W.; Li, Z.; Tan, Y.; Li, W. Optimal design and experiment on variable pacing combing brush picking device for *Lycium barbarum*. *Trans. CSAM* **2018**, *49*, 83–90. [CrossRef]
10. Zhang, W.; Zhang, M.; Zhang, J.; Li, W. Design and experiment of vibrating wolfberry harvester. *Trans. CSAM* **2018**, *49*, 97–102. [CrossRef]
11. Zhao, J.; Chen, Y.; Wang, Y.; Chen, J. Experimental research on parameter optimization of portable vibrating and harvesting device of Chinese wolfberry. *J. Agric. Mech. Res.* **2019**, *41*, 176–182. [CrossRef]
12. Wang, Y. Research on Key Technology of Wolfberry Vibration Harvest. Master's Thesis, Northwest A&F University, Yangling, China, 2018.
13. Zhou, B.; He, J. Design of simulate hand wolfberry picking machine. *Trans. CSAE* **2010**, *26* (Supp. 1), 13–17. [CrossRef]
14. He, M.; Kan, Z.; Li, C.; Wang, L.; Yang, L.; Wang, Z. Mechanism analysis and experiment on vibration harvesting of wolfberry. *Trans. CSAE* **2017**, *33*, 47–53. [CrossRef]
15. Zhao, J.; Sugirbay, A.; Liu, F.; Chen, Y.; Hu, G.; Zhang, E.; Chen, J. Parameter optimization of winnowing equipment for machineharvested *Lycium barbarum* L. *Span. J. Agric. Res.* **2019**, *17*, e0203. [CrossRef]
16. Gilman, E.F. Branch-to-stem diameter ratio affects strength of attachment. *J. Arboric.* **2003**, *29*, 291–293.
17. Kane, B.; Farrell, R.; Zedaker, S.M.; Loferski, J.R.; Smith, D.W. Failure mode and prediction of the strength of branch attachments. *Arboric. Urban For.* **2008**, *34*, 308–316. Available online: https://www.researchgate.net/profile/Brian-Kane/publication/238757178_Failure_Mode_and_Prediction_of_the_Strength_of_Branch_Attachments/links/00b7d536b533e75fc5000000/Failure-Mode-and-Prediction-of-the-Strength-of-Branch-Attachments.pdf (accessed on 25 May 2021).
18. Li, J.; Karkee, M.; Zhang, Q.; Xiao, K.; Feng, T. Characterizing apple picking patterns for robotic harvesting. *Comput. Electron. Agric.* **2016**, *127*, 633–640. [CrossRef]
19. Davidson, J.; Silwal, A.; Karkee, M.; Mo, C.; Zhang, Q. Hand-picking dynamic analysis for undersensed robotic apple harvesting. *Trans. ASABE* **2016**, *59*, 745–758. [CrossRef]
20. Slater, D.; Ennos, A.R. Determining the mechanical properties of hazel forks by testing their component parts. *Trees* **2013**, *27*, 1514–1524. [CrossRef]
21. Viet, D.D.; Ma, T.; Inagaki, T.; Kim, N.T.; Chi, N.Q.; Tsuchikawa, S. Physical and Mechanical Properties of Fast Growing Polyploid Acacia Hybrids (*A. auriculiformis* × *A. mangium*) from Vietnam. *Forests* **2020**, *11*, 717. [CrossRef]
22. Celik, H.K. Determination of bruise susceptibility of pears (Ankara variety) to impact load by means of FEM-based explicit dynamics simulation. *Postharvest Biol. Tec.* **2017**, *128*, 83–97. [CrossRef]
23. Shen, C.; Chen, Q.; Li, X.; Zhang, B.; Huang, J.; Tian, K. Test and analysis of axial compressive mechanical properties for ramie stalk. *Acta Agric. Univ. Zhejiangensis* **2016**, *28*, 688–692. [CrossRef]
24. The Poisson's Ratio. Available online: https://baike.baidu.com/item/%E6%B3%8A%E6%9D%BE%E6%AF%94/5920115?fr=aladdin (accessed on 25 May 2021).
25. Shen, C.; Li, X.; Tian, K.; Zhang, B.; Huang, J.; Chen, Q. Experimental analysis on mechanical model of ramie stalk. *Trans. CSAE* **2015**, *31*, 26–33. [CrossRef]
26. Wang, Y. *Abaqus Analysis User's Guide: Materials Volume*, 1st ed.; China Machine Press: Beijing, China, 2018; pp. 27–28.
27. Shi, N. Peeling Method of Cotton Stalk and Development of Rubbing Peeling Machine. Ph.D. Thesis, Northwest A&F University, Yangling, China, 2018.
28. Wu, J.; Huang, Y.; Wang, Y.; Wang, W. Study on axial compression properties of cotton stalks. *J. Agric. Mech. Res.* **2004**, *26*, 148–149, 152. [CrossRef]
29. Wang, Y.; Su, P. Research of mechanics characteristics for cotton stalks compression. *J. Agric. Mech. Res.* **2006**, *28*, 171–172. [CrossRef]
30. The State General Administration of Quality Supervision, Inspection and Quarantine of the People's Republic of China; China National Standardization Administration Commission. *Test Method for Flexural Properties of Sandwich Constructions*; National standards of the People's Republic of China: Beijing, China, 2005; pp. 1–9.
31. Hu, G.; Bu, L.; Chen, J. Simulation to determination of significant parameters on apple stress for combing harvesting in trellis trained trees. *Sci. Hortic.* **2020**, *274*, 109654. [CrossRef]
32. Bu, L.; Hu, G.; Chen, C.; Sugirbay, A.; Chen, J. Experimental and simulation analysis of optimum picking patterns for robotic apple harvesting. *Sci. Hortic.* **2020**, *261*, 108937. [CrossRef]